Intercalated vs non-intercalated morphologies in donor-acceptor bulk heterojunction solar cells: PBTTT:fullerene charge generation and recombination revisited

Elisa Collado-Fregoso[1,4], Samantha N. Hood[2], Safa Shoaee[1], Bob C. Schroeder[3,4], Iain McCulloch[4,5], Ivan Kassal[2,6], Dieter Neher[1] and James R. Durrant[4,7*]*

[1]Department of Physics and Astronomy, University of Potsdam, Karl-Liebknecht-Straße 24–25,14476 Potsdam-Golm, Germany

[2]Centre for Engineered Quantum Systems, School of Mathematics and Physics, The University of Queensland, QLD 4072, Australia.

[3]Materials Research Institute and School of Biological and Chemical Sciences, Queen Mary University of London, Mile End Road, London E1 4NS, United Kingdom

[4]Centre for Plastic Electronics, Department of Chemistry, Imperial College London, Exhibition Road, London SW7 2AZ, United Kingdom

[5]KSC, King Abdullah University of Science and Technology, Thuwal 23955-6900, Saudi Arabia

[6]Centre for Engineered Quantum Systems, Australian Institute for Nanoscale Science and Technology, and School of Chemistry, The University of Sydney, NSW 2006, Australia

[7]SPECIFIC IKC, College of Engineering, Swansea University, SA12 7AX, U.K.

KEYWORDS. Organic photovoltaics, bulk-heterojunction, PBTTT, charge recombination, interface nanostructure, spectroscopy.

ABSTRACT. In this contribution, we study the role of the donor:acceptor interface nanostructure upon charge separation and recombination in organic photovoltaic devices and blend films, using mixtures of PBTTT and two different fullerene derivatives ($PC_{70}BM$ and ICTA) as models for intercalated and non-intercalated morphologies, respectively. Thermodynamic simulations show that while the completely intercalated system exhibits a large free-energy barrier for charge separation, this barrier is significantly lower in the non-intercalated system, and almost vanishes when energetic disorder is included in the model. In accordance with this prediction, time-delayed collection field (TDCF) measurements reveal a pronounced field dependence of free charge generation for the completely intercalated 1:1 PBTTT:$PC_{70}BM$ but not for the fully non-intercalated 1:1 PBTTT:ICTA blend. Despite these differences, both fs-resolved transient absorption spectroscopy (TAS) and TDCF exhibit extensive first-order losses, suggesting that geminate pairs are the primary product of photoexcitation. Interestingly, the nature of these bound charges is different in these two systems, namely, coulombically bound electron-hole pairs in the intercalated blend versus morphologically secluded geminate pairs in the non-intercalated blend. In contrast, the system that comprises a combination of fully intercalated polymer:fullerene areas and fullerene aggregated domains (1:4 PBTTT:$PC_{70}BM$), is the only one that shows slow, second-order recombination of free charges, that is weakly dependent on the electric field, resulting in devices with an overall higher short circuit current and fill factor. This study therefore provides a novel consideration of the role of the interfacial nanostructure and the nature of bound charges, and their impact upon charge generation and recombination.

TEXT. The charge separation process in organic photovoltaic blends has long been studied, however significant discrepancies remain on proposed mechanisms of free polaron generation.[1–3] Variables often cited as influencing the yield of free charges are the driving energy for charge separation,[4] the availability of excited states which support a large electron delocalisation,[5–8] the dielectric constant of the blend[9] and the mobility of the photogenerated charges.[10] All of these factors are related to the micro and nanostructure of the blend, namely, the crystallinity, domain size and purity of the blend components.[11–17] More recently, the orientation of the donor and acceptor molecules with respect to each other has been proposed as a critical nanostructure parameter,[17,18] and the polarization energy at the interface has been suggested to affect the charge separation energy barrier.[19]

It is generally accepted that a trade-off exists between the optimal microstructure for efficient exciton dissociation and that for efficient separation of the charges and their subsequent collection.[20] While molecularly intermixed regions of donor and acceptor are thought to be optimal for exciton dissociation, more pure, extended regions of either component have proven necessary for an efficient charge separation and collection.[12,20–24] In addition, the nature of the morphological distribution in the donor-acceptor interface, whether blurred with a continuous composition gradient or presenting an abrupt transition between the donor and acceptor phase, was predicted to affect the efficiency of exciton harvesting and charge extraction, thus impacting upon the overall device performance.[22,25,26] A key uncertainty in such analyses is the nature of the interfacial bound charges in such bulk heterojunction (BHJ) devices and their impact upon charge generation and recombination.

In this paper, we provide a combined experimental and theoretical study of the role of the interface nanostructure upon charge separation and recombination energetics and kinetics. We

show, for the first time, that charge recombination as obtained from TAS in blends and from TDCF in devices is consistent in systems with efficient charge separation. Our study employs the prototypical polymer PBTTT (Poly[2,5-bis(3-tetradecylthiophen-2-yl)thieno[3,2-b]thiophene] blended with different loadings of $PC_{70}BM$ ([6,6]-Phenyl C71 butyric acid methyl ester) and with a bulky acceptor, ICTA (indene-C60 trisadduct, see the chemical structures and UV-vis of the neat and blend films used herein in Figure S1). The critical difference between these blends is that they give rise to very particular interfacial nanostructures.[27–30] The 1:1 PBTTT:$PC_{70}BM$ blend comprises fully intermixed polymer:fullerene co-crystals with a molecular interface, this system will be referred here as 'intercalated'. The 1:1 PBTTT:ICTA blend does not show intercalation, and has an abrupt interface, this system will be referred to as 'non-intercalated' and finally the 1:4 PBTTT:$PC_{70}BM$ blend presents both intercalated polymer:fullerene co-crystals and pure fullerene phases, and herein will be referred to as 'composite'.[27–30]

We find from our simulations that the free-energy of charge separation monotonically increases with increasing electron-hole distance when the PBTTT:$PC_{70}BM$ co-crystal is the predominant microstructure, meaning that photogenerated charges are unlikely to spontaneously separate at room temperature. However, this barrier is largely reduced for a non-intercalated sharp donor-acceptor interface such as the one present in PBTTT:ICTA, and almost vanishes if energetic disorder is included in the model. In agreement with this theory, time-delayed collection field (TDCF) studies reveal a pronounced electric field dependence of charge generation in the PBTTT:$PC_{70}BM$ co-crystal but not in the fully phase-separated PBTTT:ICTA blend. Surprisingly, photovoltaic devices fabricated with the latter blend perform worst among all systems studied. Our transient absorption spectroscopy (TAS) and TDCF recombination studies suggest that the non-intercalated blend, suffers from delayed first-order recombination, which we assign to

morphologically secluded geminate pairs, trapped in small and isolated ICTA domains. Importantly, geminate recombination is avoided in the 1:4 PBTTT:$PC_{70}BM$ system, the only system which comprises a combination of intercalated and pure fullerene phases. Therefore, our study highlights the importance of a multiphase morphology when aiming for efficient generation and extraction of charge in BHJ solar cells.

RESULTS AND DISCUSSION

First, we confirm the nanostructure of the active blends. Figure 1 shows the wide angle X-Ray diffraction (WAXD) results in films of neat PBTTT and blends of PBTTT:fullerene. In the 1:1 and 1:4 PBTTT:$PC_{70}BM$, the lamellar peaks shift to $q = 0.217$ Å^{-1} and $q = 0.218$ Å^{-1} corresponding to lamellar spacings of 29.0 Å and 28.8 Å respectively, compared to the 20.6 Å spacing in neat PBTTT film fabricated with the same conditions. Conversely, for the 1:1 PBTTT:ICTA systems, the peak remains at $q = 0.309$ Å^{-1} corresponding to a lamellar spacing of 20.3 Å, very close to the lamellar spacing in the neat PBTTT film. This confirms, as previously reported, that the system which contain a sufficient amount of a small fullerene, such as the 1:1 blend with $PC_{70}BM$, shows predominant intercalation.[27–30] This blend thus constitutes an ideal model system for a blend with only molecular heterojunctions, where every donor molecule neighbours an acceptor and vice versa. In contrast, that mixed with ICTA does not intercalate and therefore constitutes a model of an abrupt interface between pure phases, which we denote as a domain heterojunction.

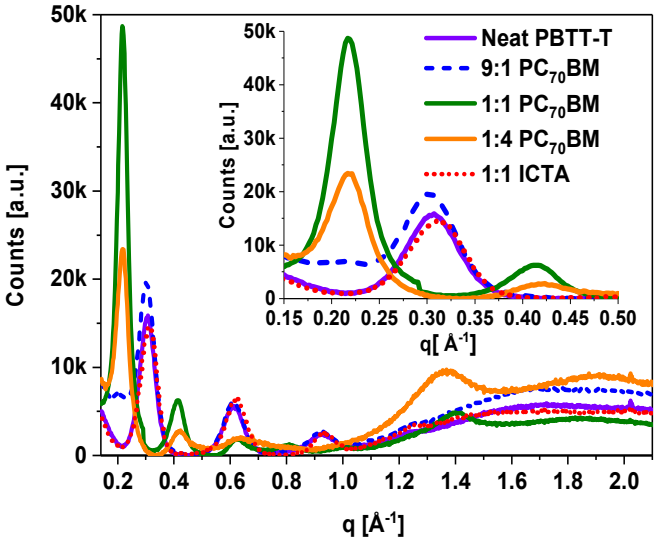

Figure 1. Wide-angle X-ray diffraction of neat PBTTT and PBTTT/fullerene thin films with different fullerene loadings.

In order to assess how the nature of the heterojunction affects the efficiency of charge generation, we performed simulations of the free energy $\Delta G(r)$ of the electron-hole pair. As we have previously described,[31] the electron and hole are initially simulated as a charge-transfer (CT) state with the hole in the PBTTT and the electron in the acceptor ($PC_{70}BM$ or ICTA).[31–33] The free energy $\Delta G(r)$ of the electron-hole pair as a function of their separation *r* is then calculated with and without energetic disorder. For the intercalated case, the PBTTT:$PC_{70}BM$ mixture is modeled as one phase with both the donor and acceptor forming one-dimensional channels, according to previous literature reports.[29,34] For the non-intercalated case, the morphology was represented as two phases of three-dimensional hexagonal close-packed lattice with a planar interface between them. Additional simulation details are described in Section 1 of the SI, including Figures S2 and S3, which show a schematic representation of the two cases.

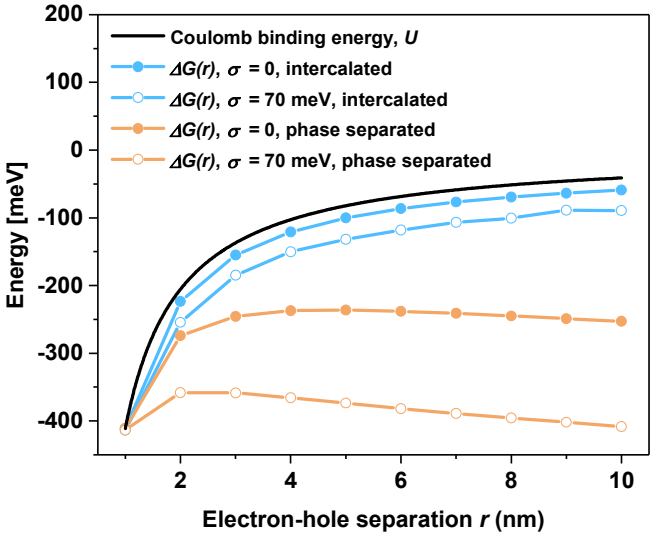

Figure 2. Electron-hole Coulombic binding (black curve) and free energy calculated without (σ = 0) and with 70 meV of a Gaussian energetic disorder for a completely intercalated morphology (full circles) and for a phase separated system (empty circles).

Figure 2 shows the results of these simulations. In the intercalated case neither entropy nor disorder have a significant effect on the free energy of dissociation. In particular, there is no entropic driving because the number of accessible states does not increase with electron-hole separation when both carriers are confined to the one-dimensional channels formed in the 1:1 PBTTT:$PC_{70}BM$ blend.[33] Conversely, for the non-intercalated case, entropy and disorder decisively lower the energetic barrier for charge-pair separation. The entropic driving comes from the fact that the number of ways of arranging two charges goes as the cube of their separation,[31] lowering the free energy. Energetic disorder also lowers the barrier by allowing charges on higher-energy sites to lower their energy by moving onto neighbouring lower-lying sites, a process that is more likely to occur in higher-dimensional systems where each site has more neighbours. In particular, we notice that using 70 meV of energetic disorder, a value estimated via Photo-CELIV

for another phase-separated system, PBTTT:bis-$PC_{60}BM$,[35] is enough to lower the charge separation barrier to ≈ 50 meV. This is a much lower energetic barrier compared to the barrier of more than 250 meV calculated for the intercalated case, independent of the presence of energetic disorder. This would suggest that charge separation is energetically more favourable in a phase separated system with a more abrupt interface. We emphasize, however, that even with a small energetic barrier, charge separation needs not be 100% efficient, since it is governed by kinetic properties that cannot be predicted from thermodynamic considerations; in particular, recombination could still be fast in phase separated blends, leading to low efficiencies.

To determine whether the predominance of non-intercalated blends results in superior device performance, charge generation and recombination were studied in detail with a combination of different steady-state and transient methods. Figure 3 shows the *J-V* curves of the PBTTT:fullerene devices (see Table 1 in the SI for the device parameters) along with the external generation efficiency (EGE) obtained from our TDCF measurements, described elsewhere.[36,37] Briefly, a 3.8 ns monochromatic (here 532 nm) light pulse was shined into the device pixel while the device is held at a certain bias ('pre-bias' V_{pre}); after a certain delay time, the charges are extracted using a strong reverse bias ('collection bias' V_{coll}). EGE is calculated as the ratio of total charge carrier collected per photons shined. Data in Figure 3 is obtained by keeping the delay constant at the earliest time (6 ns) and lowest measurable intensity, (0.2 μJcm^2) while the pre-bias is changed, using a collection bias $V_{coll} = -2.5\ V$.

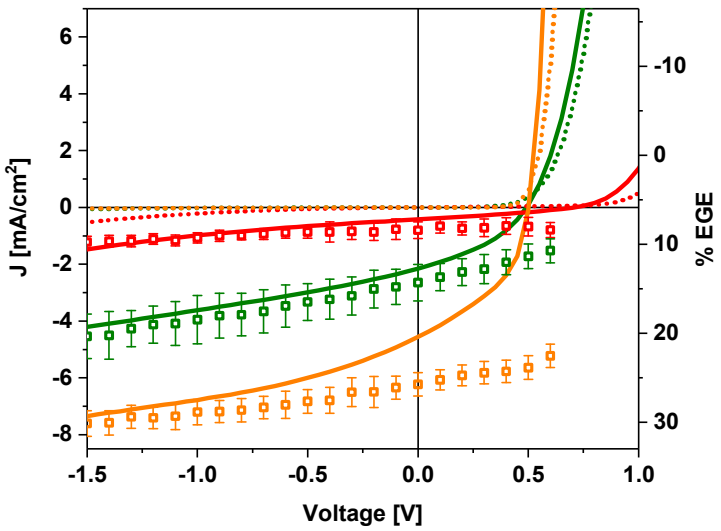

Figure 3. *J-V* curves of representative, bulk heterojunction devices (ITO/PEDOT:PSS/active blend/Ca/Al) under constant, 100 mWcm^{-2}, AM 1.5 spectrum from a solar simulated light at room temperature. The active blends are composed of: (w/w) 1:4 PBTTT/$PC_{70}BM$ (orange curve), 1:1 PBTTT/$PC_{70}BM$ (green curve) and 1:1 PBTTT/ICTA (red curve). Dotted lines correspond to the dark currents of the corresponding devices. Open squares represent the external generation efficiency as obtained by TDCF at 6 ns and using -2.5 V for the collection bias after excitation at 540 nm and 0.2 μJcm^2. (see text)

As can be observed, the *J-V* curves (both in shape and absolute current) are well described by our estimated EGE at reverse bias, where non-geminate charge recombination is reduced by the effect of the applied filed. This means that the device photocurrent is generated exactly by the charges measured by TDCF at short delay times. It is also evident that whereas for the intercalated device the effect of pre-bias on generation is relatively large (EGE varies from 20 to 11% from -1.5 to 0.6 V) this effect is much less pronounced for the composite device (30 to 23%) and even less for the non-intercalated device (10 to 8%). The trend for the extreme cases i.e., intercalated vs non-intercalated, are in agreement with conclusions from earlier TDCF measurements on a similar system.[38] Consistent with our simulations, this finding suggests that free charge photogeneration

in the intercalated 1:1 PBTTT:$PC_{70}BM$ device proceeds via coulombically bound intermediates – namely, charge pairs– that are bias-susceptible and extractable under strong applied bias. Conversely, the presence of relatively pure phases in the non-intercalated and composite devices results in charge separation significantly less dependent on the electric field – indicating a lower barrier for free charge formation in both systems. This is due to the formation of less bound charges or the formation bound charges that are less bias-susceptible. Later on, we will see that the last explanation seems to fit well with the evidence obtained by other measurements for the non-intercalated, PBTTT:ICTA device.

Despite the low bias influence on EGE for the PBTTT:ICTA device, it is striking how low the absolute EGE is even at -1.5 V reverse bias and how poorly this device performs, given the thermodynamic prediction of supressed geminate recombination at an abrupt domain heterojunction interface. To understand this apparent disagreement, we studied charge recombination dynamics, employing both fs-TAS and TDCF as a function of delay time. Although there have been several spectroscopic studies of PBTTT systems varying the amount of intermixed regions,[21,30,39–43] a detailed analysis of charge kinetics in both blends and working solar devices where the interfacial nanostructure is controlled has been lacking.

Figure S4 shows the fs-TAS spectra and kinetics of a neat PBTTT film and a 9:1 PBTTT:$PC_{70}BM$ blend film. From these data, the singlet exciton photoinduced absorption band, with a maximum at 1260 nm can be identified.[21] Its lifetime is estimated (at low intensity) to be $\tau = 144 \pm 20$ ps, consistent with the lifetime of other conjugated polymers used in organic photovoltaics.[44] The band appearing from ≈ 850 to 1050 nm for the 9:1 blend can be assigned to the photoinduced absorption of bound/free positive polarons in the polymer phase, consistent with other reports.[21,40,43,42] These are the basis of the assignments that will be used for the rest of the

blends herein presented. Using the exciton photoinduced absorption kinetics for the neat PBTTT film at different excitation intensities and a modified time-independent exciton-exciton annihilation model,[45,23] we can estimate the one-dimensional polymer exciton diffusion length L_{exc} to be ≈ 7 nm. By quantifying the exciton lifetime for the different blend films at the band maximum and comparing it with the steady-state photoluminescence (PL) results (Figure S5) we can obtain a value for the polymer PL quenching, which, along with the polymer exciton diffusion length, can give an estimate of the pure domain size.[11,23,24,46]

We now turn to Figure 4. Here we show, on the left column the transient spectra of the blend films. On the middle column the normalized TAS kinetics at the maximum of the bound/free polaron pairs (≈ 1000 nm for the $PC_{70}BM$ blends and 930 nm for the ICTA blend) and on the right one the corresponding normalized kinetics of total charge density obtained by TDCF at $V_{pre} = 0.4\ V$ (near V_{OC}). As is evident in panels a and d for the 1:1 and 1:4 PBTTT:$PC_{70}BM$ blends, the exciton photoinduced absorption band is scarcely present, indicating that exciton dissociation occurs on ultrafast times, (≤ 200 fs) in agreement with previous studies,[21,40,42,43] and consistent with the presence of completely intercalated areas. We note however, that this is not the case for the ICTA blend, where the exciton band is present, (see panel g) consistent with the idea that this blend has some degree of phase separation, with slower, exciton diffusion-limited charge generation kinetics (panel h). Figure S6 shows in panel d the decay kinetics of the PBTTT:ICTA blend exciton photoinduced absorption, from where an average lifetime of $\tau = 3.5 \pm 0.6$ ps for exciton dissociation was obtained from a tri-exponential fit. We remark however, that from our estimation of the polymer exciton dissociation length in the neat PBTTT film, and the exciton lifetime in the ICTA blend, pure polymer domains have an average diameter of 2 nm. This

indicates that despite the inability of ICTA to intercalate and form a co-crystal with PBTTT, the size of the pure polymer domains in its blend is fairly small.

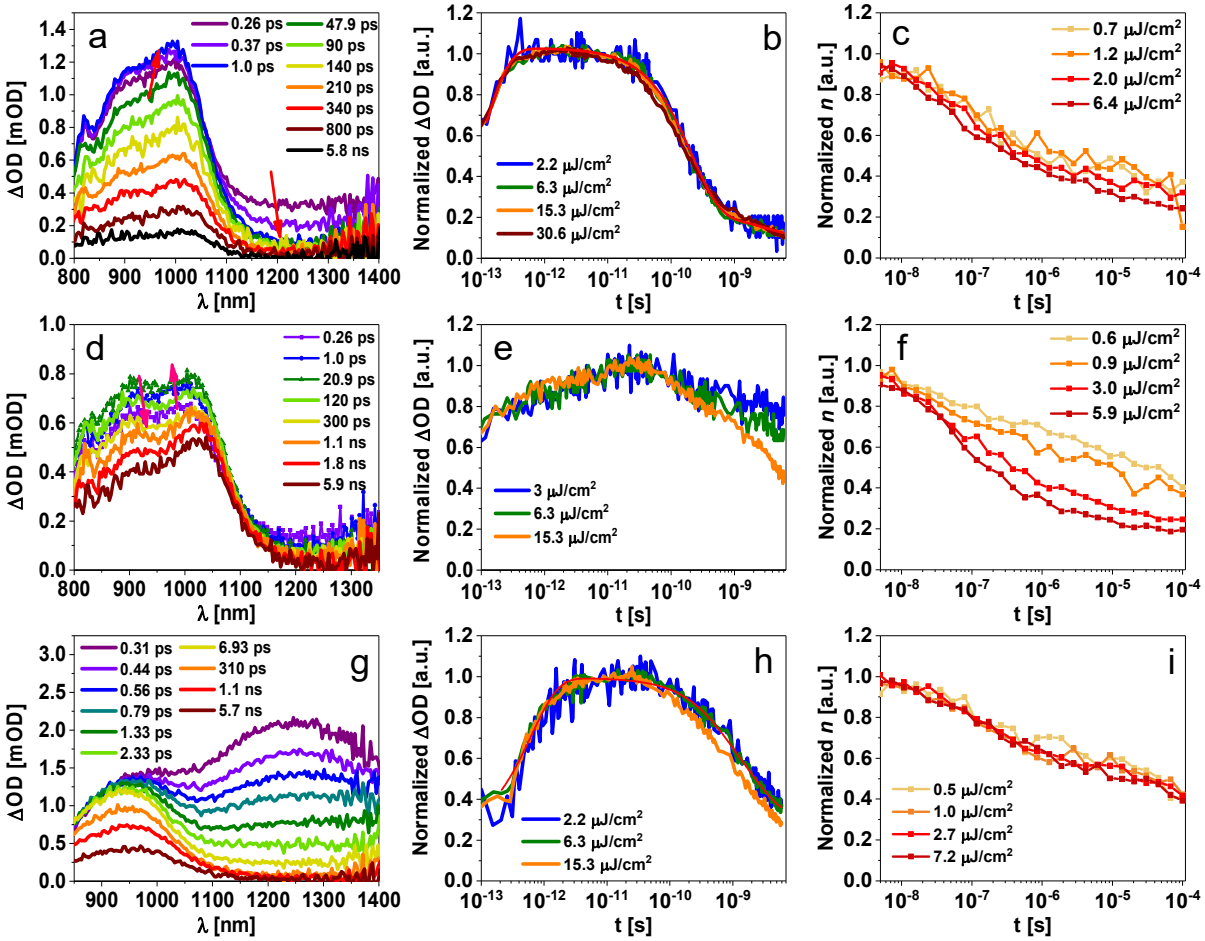

Figure 4. The three studied systems, one in each row: (a, b, c) 1:1 PBTTT:$PC_{70}BM$, (d, e, f) 1:4 PBTTT:$PC_{70}BM$ and (g, h, i) 1:1 PBTTT:ICTA. Columns show: (a, d, g) plots of transient absorption (TAS) spectra exciting at 540 nm with 6 μJ/cm^2, (b, e, h) normalized polaron recombination kinetics from TAS at the absorption maximum, at different excitation intensities; and (c, f, i) normalized charge density from time-delayed collection field (TDCF) measurements at 0.4 V prebias and different light pulse intensities. Red lines in plot b and h correspond to tri-exponential fits of the data. Plot g) shows the raw TAS spectra before subtracting exciton photoinduced absorption, which is included in the SI. Plot h) shows deconvoluted polaron kinetics co (exciton contribution has been substracted).

Now we discuss the decay dynamics of the photogenerated charges in the blends and devices. Only the 1:4 PBTTT:$PC_{70}BM$ blend shows clear intensity-dependent decays, which start at ≈ 10 ps, and exhibit a half time of ~ 4 ns at the highest intensity study. This intensity dependent behaviour is also present in the total charge density on the ns timescale measured with TDCF, where a much faster decay is observed when the pulse intensity is increased by a factor of 10. From the fits of these decays (not shown) a predominant second order kinetics can be obtained.

The scenario is completely different for the 1:1 PBTTT:$PC_{70}BM$ (intercalated) and PBTTT:ICTA (non-intercalated) systems. In the first case, a fast intensity-independent decay of the polaron absorption is observed. This decay can be fitted to an exponential decay with an average time constant of $\tau = 210 \pm 10$ ps. After ~ 2 ns 80% of the charges are lost to this fast charge recombination, in agreement with other studies.[21,40,42,43] The TDCF data also show an intensity-independent first-order recombination process, in agreement with ns-TAS measurements by Laquai et al.[21] Our external quantum efficiency (EQE) measurements in the near IR (see Figure S7) show a band at ~ 980 nm, which suggests that there are bound species with an absorption coupled to the ground state that can generate free charges. These species therefore correspond to charge-transfer states. We envision that recombination of the most tightly bound states results in fast geminate recombination that starts from early times, leaving the loosely bound polaron pairs to survive recombination at longer time scales, and being more prone to be separated and extracted by a sufficiently large bias.

For the non-intercalated PBTTT:ICTA system, for which our simulations predict efficient free charge generation, the polaron TAS decays are surprisingly intensity-independent; however they

undergo an exponential decay with a much larger time constant, ($\tau = 1.8 \pm 0.2$ ns) compared with the fully intercalated system. Importantly, charge recombination follows a first order decay also in TDCF, while charge extraction is rather slow (see Figure S8). An important relatively slow rise of the signal with a time constant of $\tau = 0.60 \pm 0.1$ ps is also observed. This corresponds to a fraction of polaron pairs that are generated after exciton diffusion from pure polymer areas to the interface (see Figure S1). The slower rise (as opposed to that of the composite 1:1 PBTTT:$PC_{70}BM$ blend) suggests that PBTTT domains are somewhat larger, in agreement with steady-state PL. Interestingly, our EQE measurements do not show the presence of any near-IR absorption (see Figure S7) indicating that if there are bound species, they are not coupled to the ground state. This evidence suggests that exciton dissociation at the abrupt interface indeed forms charge pairs with a minimum separation distance to lower their free energy (see Figure 2), but that they remain morphologically confined in small polymer or fullerene domains, with only few percolation pathways being available to be extracted. In this scenario, a large fraction of electron-hole pairs located on neighbouring domains will not be able to separate into fully independent charge carriers and thus geminately recombine. Consequently, charge recombination is first order in carrier density, but more gradual and slower than in the intercalated blend where geminate pairs are forced to recombine due to the presence of a large and deep energy barrier (see Figure 2 and Scheme 1).

This study reveals important differences in the charge carrier dynamics of PBTTT:fullerene blends depending on the heterojunction morphology and domain purity. For the 1:1 PBTTT:$PC_{70}BM$ blend, with an intercalated morphology, our simulations and TDCF data show free carrier formation to proceed through a (coulombically) bound precursor. However, as there are no internal domain boundaries, carriers can be efficiently extracted to the outside circuit with the assistance of an electric field. In agreement with this picture, geminate, first order polaron

recombination dominates the kinetics in the absence of an electric field (like in TAS or TDCF near V_{OC}), but there is a noticeable increase of the EGE when reversing the bias, thus rendering a strong voltage-dependent photocurrent. These observations are consistent with a recent semi-empirical theoretical study of the effect of intermixed regions upon charge recombination.[26] In contrast, in the non-intercalated 1:1 PBTTT:ICTA system, there is a shallow energetic barrier to separate the interfacial CT state, and yet most of the photogenerated charge pairs are morphologically bound. As a consequence, polaron recombination as obtained by TAS is first order, and the EGE remains at a low level independently of the applied voltage. An additional factor that can contribute to the poor charge separation and collection in the 1:1 PBTTT:ICTA device may originate from the expected lower charge mobility of ICTA, as compared to $PC_{70}BM$,[47] which can hinder efficient charge generation and collection.[10]

It is only in the 1:4 PBTT:$PC_{70}BM$ system, with a composite morphology, that the majority of photogenerated polarons fully separate, then exhibiting slow, second order recombination dynamics, and an overall higher EGE. We propose that in this system, charge separation benefits from the presence of larger and well-interconnected fullerene domains. It is also plausible that an energy cascade effect operates in the junction between the co-crystal and the semi-crystallized $PC_{70}BM$ areas with higher-electron-affinity.[11,48] This is an effect unlikely to be present in the ICTA blends due to their small and non-crystallized domains, as can be observed in the WAXD data which does not show the characteristic peak at q = 1.37 $Å^{-1}$, proposed to come from aggregated fullerene areas.[49,50] Note that this peak is only present for the 1:4 PBTTT:$PC_{70}BM$ blend where larger $PC_{70}BM$ domains are present.[29,30]

A second important conclusion comes from the direct comparison of TAS and TDCF data in Scheme 1. Here, by assuming that the two measurements overlap at ≈ 6 ns, and low excitation

intensities (2.2 mJcm^{-2}) we can obtain the polymer (hole) polaron extinction coefficient ε_P from the TAS data, at the polaron maximum absorption. Using this approach, we estimate that $\varepsilon_P = (4.0 \pm 0.7) \times 10^4\ M^{-1}cm^{-1}$ for PBTTT hole polarons, which is consistent with published data for other polymers used in OPV.[51] We notice however, that this value was obtained using only the 1:1 and 1:4 PBTTT:$PC_{70}BM$ transients. Interestingly, for the 1:1 PBTTT:ICTA system, the optical and optoelectronical methods do not seem to agree in the charge density obtained: the extractable charge density determined by TDCF is ≈ 2.6 times lower than the total charge in the blend as estimated by TAS measurements. This is consistent with the idea that most of these charges are morphologically secluded, rendering them vulnerable for geminate recombination and thus difficult to move be extracted efficiently even under the influence of a strong bias. This is explicitly illustrated in the right panel of Scheme 1.

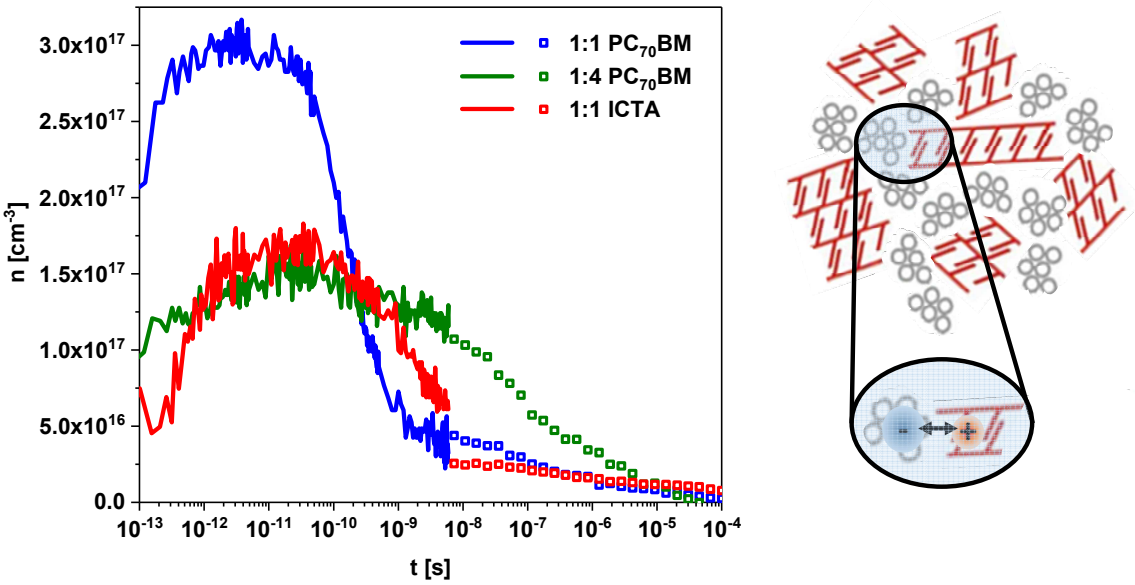

Scheme 1. Absolute charge density kinetics from TAS (lines) on thin films and TDCF (open squares) on the corresponding devices for the three studied systems using pulse excitations at 540 nm and 2.2 μJ/cm^2. A hole polaron extinction coefficient of $(4.0 \pm 0.7) \times 10^4\ M^{-1}cm^{-1}$ is

obtained The scheme at the right illustrates the proposed morphology that is believed to be present in the 1:1 PBTTT:ICTA blend and is responsible for the discrepancy observed from TAS and TDCF (see text).

Finally, it is worth noticing in Scheme 1 that "instantaneous" (≤ 200 fs) charge generation is actually more efficient in the 1:1 PBTTT:$PC_{70}BM$ system, where in the range from ≈ 200 fs to 45 ps charge density is almost 1.5 times higher than for the other two systems. However, notice that charge generation as determined by TAS does not discriminate between bound or free charges; and after ≈ 200 ps the charge density in the other two blends is higher due to their slower charge recombination. While it is important to understand the polaron pair kinetics from the ultrafast time scales, it is the free charge density at times relevant for charge extraction that is mostly relevant to device operation, differently to what has been proposed in the literature.[43]

CONCLUSION.

We have demonstrated the impact of the interface morphology upon charge generation, recombination and extraction in a joined kinetic study in blends and devices. While thermodynamic simulations show that charge separation is more efficient at an abrupt interface compared to an intercalated one, the former displays the lowest device efficiency. This is due to a kinetic inability of the non-intercalated system to form free charges in high mobility domains that favour efficient extraction. Remarkably, in both extreme cases - where either intercalated or phase-separated domains predominate - charges undergo geminate recombination of Coulombically or morphologically bound polaron pairs. In stark contrast, the composite 1:4 PBTTT:$PC_{70}BM$ system

is the only one that results in good extraction and delayed, non-geminate recombination. This indicates that both intermixed and pure phases are required for an efficient device.

METHODS. *Film preparation*. For optical measurements (fs-TAS, steady state PL) and device fabrication, solutions of PBTTT and $PC_{70}BM$ (or ICTA) in orto-dichlorobenzene (ODCB) were prepared at a concentration between 15 – 30 mg mL^{-1}. The solutions were stirred and heated at 90°C for at least 8 hours to ensure full dissolution. The films were spun on cleaned glass substrates for 1 minute at 1500 rpm. For WAXD measurements, films were prepared by drop-casting 30 mg mL^{-1} solutions of the neat polymer or the polymer/acceptor mixtures onto clean glass substrates.

Device fabrication. Pre-cleaned, patterned indium tin oxide (ITO) substrates (15 Ω per square) were used and treated with Oxygen plasma. On top of the ITO substrates, PEDOT:PSS was spun at 2500 rpm and dried on a hot plate at 150°C in air for 30 minutes. Active layers for devices were prepared in a similar fashion as for the films used for optical measurements. Following, a counter electrode of calcium (10 nm) and aluminum (100 nm) were deposited by vacuum evaporation at 3 × 10^{-7} mbar. The active area of the devices used for TDCF was 0.01 cm^2. Devices were encapsulated with blue fix glue.

Transient absorption spectroscopy (TAS): Measurements were carried out with a commercial setup that comprises a 1 kHz Solstice (Newport Corporation) Ti:Sapphire regenerative amplifier with 800 nm, 90 fs pulses. The output was passed through a beam splitter to generate the pump and probe pulses. The tuneable pump pulse was generated in a TOPAS-Prime (Light conversion) optical parametric amplifier and used to excite the sample with energies between 2 and 30 μJcm^{-2} at 540 nm. The probe light was used to generate a Near-IR continuum (800-1400 nm) in a sapphire crystal. A HELIOS transient absorption spectrometer (Ultrafast Systems) was used for collecting

transient absorption spectra and decays up to 6 ns. The time resolution of this set-up is 200 fs. The films were kept at all times under a Nitrogen atmosphere.

Time delayed collection field (TDCF). An optical pulse train generated by a diode-pumped, Q-switched Nd:YAG laser (NT242, EKSPLA, 500 Hz repetition rate, 3.8 ns pulse duration) was used to excite the sample. In the meantime, the device is held at a constant 'pre-bias' set by an Agilent 81150 A pulse generator trough a homebuilt amplifier and then switched to a strong reverse bias 'collection bias' after a certain delay time. The current through the device is measured via a grounded 10 Ω resistor in series with the sample and recorded with an Agilent DSO9104H oscilloscope. To compensate for the internal latency of the pulse generator, the laser pulse was delayed and homogeneously scattered in an 85 m long silica fiber (LEONI).

ASSOCIATED CONTENT

Supporting Information. Structures of the donor polymer and fullerene acceptors are included as well as UV-vis steady-state absorption of the respective neat and blend films. Details of the Thermodynamic simulations, optical spectroscopy (TAS and PL) complementary data. EQE and device efficiency figures and finally TDCF transient of devices are included. The Supporting Information is free of charge on the ACS Publication website.

AUTHOR INFORMATION

Corresponding Authors

*E-mail: neher@uni-potsdam.de, j.durrant@imperial.ac.uk

Author Contributions

The manuscript was written through contributions of all authors. All authors have given approval to the final version of the manuscript.

ACKNOWLEDGMENTS

This work was funded by UNVEiL, a BMBF project, the EPSRC and the Welsh Assembly Government Sêr Cymru programme. ECF thanks CONACyT (scholarship 309929) and the Kernahan Fund from Imperial College London for funding. SNH and IK were supported by the Westpac Bicentennial Foundation and by the Australian Research Council through a Discovery Early Career Researcher Award (DE140100433) and through the Centre of Excellence for Engineered Quantum Systems (CE110001013).

ABBREVIATIONS

PBTTT, Poly[2,5-bis(3-tetradecylthiophen-2-yl)thieno[3,2-b]thiophene]; $PC_{70}BM$, [6,6]-Phenyl C71 butyric acid methyl ester; ICTA, indene-C60 trisadduct; TAS, fs-Transient absorption spectroscopy; TDCF, Time-delayed collection field; Photo-CELIV, Charge Extraction by Linearly Increasing Voltage; EGE, External generation efficiency V_{pre}, Pre-bias; V_{coll}, Collection bias; L_{exc}, Exciton diffusion length; PL, steady-state Photoluminescence; EQE, External quantum efficiency, ε_P, Polaron extinction coefficient.

REFERENCES

(1) Gao, F.; Inganas, O. Charge Generation in Polymer–fullerene Bulk-Heterojunction Solar Cells. *Phys. Chem. Chem. Phys.* **2014**, *16*, 20291–20304.

(2) Few, S.; Frost, M.; Nelson, J. Models of Charge Pair Generation in Organic Solar Cells. *Phys. Chem. Chem. Phys.* **2014**, *17*, 2311–2325.

(3) Bässler, H.; Köhler, A. “Hot or Cold”: How Do Charge Transfer States at the Donor–

acceptor Interface of an Organic Solar Cell Dissociate? *Phys. Chem. Chem. Phys.* **2015**, *17* (43), 28451–28462.

(4) Dimitrov, S. D.; Durrant, J. R. Materials Design Considerations for Charge Generation in Organic Solar Cells. *Chem. Mater.* **2013**, *26*, 616–630.

(5) Bakulin, A. a; Rao, A.; Pavelyev, V. G.; van Loosdrecht, P. H. M.; Pshenichnikov, M. S.; Niedzialek, D.; Cornil, J.; Beljonne, D.; Friend, R. H. The Role of Driving Energy and Delocalized States for Charge Separation in Organic Semiconductors. *Science* **2012**, *335*, 1340–1344.

(6) Savoie, B. M.; Rao, A.; Bakulin, A. A.; Gelinas, S.; Movaghar, B.; Friend, R. H.; Marks, T. J.; Ratner, M. A. Unequal Partnership: Asymmetric Roles of Polymeric Donor and Fullerene Acceptor in Generating Free Charge. *J. Am. Chem. Soc.* **2014**, *136* (7), 2876–2884.

(7) Niedzialek, D.; Duchemin, I.; de Queiroz, T. B.; Osella, S.; Rao, A.; Friend, R.; Blase, X.; Kümmel, S.; Beljonne, D. First Principles Calculations of Charge Transfer Excitations in Polymer-Fullerene Complexes: Influence of Excess Energy. *Adv. Funct. Mater.* **2015**, *25*, 1972–1984.

(8) Jones, M. L.; Dyer, R.; Clarke, N.; Groves, C. Are Hot Charge Transfer States the Primary Cause of Efficient Free-Charge Generation in Polymer:fullerene Organic Photovoltaic Devices? A Kinetic Monte Carlo Study. *Phys. Chem. Chem. Phys.* **2014**, *16* (38), 20310–20320.

(9) Bernardo, B.; Cheyns, D.; Verreet, B.; Schaller, R. D.; Rand, B. P.; Giebink, N. C. Delocalization and Dielectric Screening of Charge Transfer States in Organic Photovoltaic Cells. *Nat. Commun.* **2014**, *5*, 3245.

(10) Philippa, B.; Stolterfoht, M.; Burn, P. L.; Juška, G.; Meredith, P.; White, R. D.; Pivrikas, A. The Impact of Hot Charge Carrier Mobility on Photocurrent Losses in Polymer-Based Solar Cells. *Sci. Rep.* **2014**, *4*, 5695.

(11) Jamieson, F. C.; Domingo, E. B.; McCarthy-Ward, T.; Heeney, M.; Stingelin, N.; Durrant, J. R. Fullerene Crystallisation as a Key Driver of Charge Separation in Polymer/fullerene Bulk Heterojunction Solar Cells. *Chem. Sci.* **2012**, *3* (2), 485.

(12) Shoaee, S.; Subramaniyan, S.; Xin, H.; Keiderling, C.; Tuladhar, P. S.; Jamieson, F.; Jenekhe, S. A.; Durrant, J. R. Charge Photogeneration for a Series of Thiazolo-Thiazole Donor Polymers Blended with the Fullerene Electron Acceptors PCBM and ICBA. *Adv. Funct. Mater.* **2013**, *23* (26), 3286–3298.

(13) Ma, W.; Tumbleston, J. R.; Wang, M.; Gann, E.; Huang, F.; Ade, H. Domain Purity, Miscibility, and Molecular Orientation at Donor/acceptor Interfaces in High Performance Organic Solar Cells: Paths to Further Improvement. *Adv. Energy Mater.* **2013**, *3* (7), 864–872.

(14) Vandewal, K.; Himmelberger, S.; Salleo, A. Structural Factors That Affect the Performance

of Organic Bulk Heterojunction Solar Cells. *Macromolecules* **2013**, *46* (16), 6379–6387.

(15) Mukherjee, S.; Proctor, C. M.; Bazan, G. C.; Nguyen, T.; Ade, H. Signifi Cance of Average Domain Purity and Mixed Domains on the Photovoltaic Performance of High-Effi Ciency Solution-Processed Small-Molecule BHJ Solar Cells. *Adv. Energy Mater.* **2015**, *5*, 1500877.

(16) Mukherjee, S.; Jiao, X.; Ade, H. Charge Creation and Recombination in Multi-Length Scale Polymer:Fullerene BHJ Solar Cell Morphologies. *Adv. Energy Mater.* **2016**, *6* (18), 1–8.

(17) Jiao, X.; Ye, L.; Ade, H. Quantitative Morphology-Performance Correlations in Organic Solar Cells: Insights from Soft X-Ray Scattering. *Adv. Energy Mater.* **2017**, *1700084*, 1700084.

(18) Tumbleston, J. R.; Collins, B. a.; Yang, L.; Stuart, A. C.; Gann, E.; Ma, W.; You, W.; Ade, H. The Influence of Molecular Orientation on Organic Bulk Heterojunction Solar Cells. *Nat. Photonics* **2014**, *8* (5), 385–391.

(19) Ryno, S. M.; Fu, Y. T.; Risko, C.; Bredas, J. L. Polarization Energies at Organic-Organic Interfaces: Impact on the Charge Separation Barrier at Donor-Acceptor Interfaces in Organic Solar Cells. *ACS Appl. Mater. Interfaces* **2016**, *8* (24), 15524–15534.

(20) Kästner, C.; Egbe, D. A. M.; Hoppe, H. Polymer Aggregation Control in Polymer–fullerene Bulk Heterojunctions Adapted from Solution. *J. Mater. Chem. A* **2015**, *3* (1), 395–403.

(21) Gehrig, D. W.; Howard, I. A.; Sweetnam, S.; Burke, T. M.; Mcgehee, M. D.; Laquai, F. The Impact of Donor – Acceptor Phase Separation on the Charge Carrier Dynamics in pBTTT : PCBM Photovoltaic Blends. *Macromol. Rapid Commun.* **2015**, *36*, 1054–1060.

(22) Yan, H.; Song, Y.; McKeown, G. R.; Scholes, G. D.; Seferos, D. S. Adding Amorphous Content to Highly Crystalline Polymer Nanowire Solar Cells Increases Performance. *Adv. Mater.* **2015**, *27* (23), 3484–3491.

(23) Collado-Fregoso, E.; Deledalle, F.; Utzat, H.; Tuladhar, P. S.; Dimitrov, S. D.; Gillett, A.; Tan, C. H.; Zhang, W.; McCulloch, I.; Durrant, J. R. Photophysical Study of DPPTT-T/PC70BM Blends and Solar Devices as a Function of Fullerene Loading: An Insight into EQE Limitations of DPP-Based Polymers. *Adv. Funct. Mater.* **2017**, *27* (6), 1–11.

(24) Utzat, H.; Dimitrov, S. D.; Wheeler, S.; Collado-Fregoso, E.; Tuladhar, P. S.; Schroeder, B. C.; McCulloch, I.; Durrant, J. R. Charge Separation in Intermixed Polymer:PC70BM Photovoltaic Blends: Correlating Structural and Photophysical Length Scales as a Function of Blend Composition. *J. Phys. Chem. C* **2017**, *121* (18), 9790–9801.

(25) Lyons, B. P.; Clarke, N.; Groves, C. The Relative Importance of Domain Size, Domain Purity and Domain Interfaces to the Performance of Bulk-Heterojunction Organic Photovoltaics. *Energy Environ. Sci.* **2012**, *5* (6), 7657.

(26) Finck, B. Y.; Schwartz, B. J. Drift-Diffusion Studies of Compositional Morphology in Bulk Heterojunctions: The Role of the Mixed Phase in Photovoltaic Performance. *Phys. Rev. Appl.* **2016**, *6* (5), 1–16.

(27) Miller, N. C.; Sweetnam, S.; Hoke, E. T.; Gysel, R.; Miller, C. E.; Bartelt, J. A.; Xie, X.; Toney, M. F.; McGehee, M. D. Molecular Packing and Solar Cell Performance in Blends of Polymers with a Bisadduct Fullerene. *Nano Lett.* **2012**, *12* (3), 1566–1570.

(28) Miller, N. C.; Cho, E.; Gysel, R.; Risko, C.; Coropceanu, V.; Miller, C. E.; Sweetnam, S.; Sellinger, A.; Heeney, M.; McCulloch, I.; Brédas, J. L.; Toney, M. F.; McGehee, M. D. Factors Governing Intercalation of Fullerenes and Other Small Molecules between the Side Chains of Semiconducting Polymers Used in Solar Cells. *Adv. Energy Mater.* **2012**, *2* (10), 1208–1217.

(29) Miller, N. C.; Cho, E.; Junk, M. J. N.; Gysel, R.; Risko, C.; Kim, D.; Sweetnam, S.; Miller, C. E.; Richter, L. J.; Kline, R. J.; Heeney, M.; McCulloch, I.; Amassian, A.; Acevedo-Feliz, D.; Knox, C.; Hansen, M. R.; Dudenko, D.; Chmelka, B. F.; Toney, M. F.; Brédas, J. L.; McGehee, M. D. Use of X-Ray Diffraction, Molecular Simulations, and Spectroscopy to Determine the Molecular Packing in a Polymer-Fullerene Bimolecular Crystal. *Adv. Mater.* **2012**, *24* (45), 6071–6079.

(30) Buchaca-Domingo, E.; Ferguson, a. J.; Jamieson, F. C.; McCarthy-Ward, T.; Shoaee, S.; Tumbleston, J. R.; Reid, O. G.; Yu, L.; Madec, M.-B.; Pfannmöller, M.; Hermerschmidt, F.; Schröder, R. R.; Watkins, S. E.; Kopidakis, N.; Portale, G.; Amassian, a.; Heeney, M.; Ade, H.; Rumbles, G.; Durrant, J. R.; Stingelin, N. Additive-Assisted Supramolecular Manipulation of Polymer:fullerene Blend Phase Morphologies and Its Influence on Photophysical Processes. *Mater. Horizons* **2014**, *1* (2), 270.

(31) Hood, S. N.; Kassal, I. Entropy and Disorder Enable Charge Separation in Organic Solar Cells. *J. Phys. Chem. C* **2016**, *7*, 4495–4500.

(32) Clarke, T. M.; Durrant, J. R. Charge Photogeneration in Organic Solar Cells. *Chem. Rev.* **2010**, *110*, 6736–6767.

(33) Gregg, B. A. Entropy of Charge Separation in Organic Photovoltaic Cells: The Benefit of Higher Dimensionality. *J. Phys. Chem. Lett.* **2011**, *2* (24), 3013–3015.

(34) Poelking, C.; Cho, E.; Malafeev, A.; Ivanov, V.; Kremer, K.; Risko, C.; Brédas, J. L.; Andrienko, D. Characterization of Charge-Carrier Transport in Semicrystalline Polymers: Electronic Couplings, Site Energies, and Charge-Carrier Dynamics in Poly(bithiophene-Alt-Thienothiophene) [PBTTT]. *J. Phys. Chem. C* **2013**, *117* (4), 1633–1640.

(35) Nyman, M.; Sandberg, O. J.; Österbacka, R. Charge Transport in Intercalated and Non-Intercalated Polymer:fullerene Blends. *Synth. Met.* **2015**, *201*, 6–10.

(36) Kniepert, J.; Schubert, M.; Blakesley, J.; Neher, D. Photogeneration and Recombination in P3HT : PCBM Solar Cells Probed by Time Delayed Collection Field Experiments. *J. Phys. Chem. Lett.* **2011**, 700–705.

(37) Kurpiers, J.; Neher, D. Dispersive Non-Geminate Recombination in an Amorphous Polymer:Fullerene Blend. *Sci. Rep.* **2016**, *6* (1), 26832.

(38) Zusan, A.; Vandewal, K.; Allendorf, B.; Hansen, N. H.; Pfl, J.; Salleo, A.; Dyakonov, V.;

Deibel, C. The Crucial Influence of Fullerene Phases on Photogeneration in Organic Bulk Heterojunction Solar Cells. *Adv. Energy Mater.* **2014**, *4*, 1400922.

(39) Rance, W. L.; Ferguson, A. J.; McCarthy-Ward, T.; Heeney, M.; Ginley, D. S.; Olson, D. C.; Rumbles, G.; Kopidakis, N. Photoinduced Carrier Generation and Decay Dynamics in Intercalated and Non-Intercalated Polymer:fullerene Bulk Heterojunctions. *ACS Nano* **2011**, *5* (7), 5635–5646.

(40) Scarongella, M.; Paraecattil, A. A.; Buchaca-Domingo, E.; Douglas, J. D.; Beaupré, S.; McCarthy-Ward, T.; Heeney, M.; Moser, J.-E.; Leclerc, M.; Fréchet, J. M. J.; Stingelin, N.; Banerji, N. The Influence of Microstructure on Charge Separation Dynamics in Organic Bulk Heterojunction Materials for Solar Cell Applications. *J. Mater. Chem. A* **2014**, *2* (17), 6218–6230.

(41) Dou, F.; Buchaca-Domingo, E.; Sakowicz, M.; Rezasoltani, E.; McCarthy-Ward, T.; Heeney, M.; Zhang, X.; Stingelin, N.; Silva, C. The Effect of Phase Morphology on the Nature of Long-Lived Charges in Semiconductor Polymer:fullerene Systems. *J. Mater. Chem. C* **2015**, *3* (15), 3722–3729.

(42) Scarongella, M.; De Jonghe-Risse, J.; Buchaca-Domingo, E.; Causa, M.; Fei, Z.; Heeney, M.; Moser, J. E.; Stingelin, N.; Banerji, N. A Close Look at Charge Generation in Polymer: Fullerene Blends with Microstructure Control. *J. Am. Chem. Soc.* **2015**, *137* (8), 2908–2918.

(43) Causa, M.; De Jonghe-Risse, J.; Scarongella, M.; Brauer, J. C.; Buchaca-Domingo, E.; Moser, J.-E.; Stingelin, N.; Banerji, N. The Fate of Electron–hole Pairs in Polymer:fullerene Blends for Organic Photovoltaics. *Nat. Commun.* **2016**, *7*, 12556.

(44) Dimitrov, S.; Schroeder, B.; Nielsen, C.; Bronstein, H.; Fei, Z.; McCulloch, I.; Heeney, M.; Durrant, J. Singlet Exciton Lifetimes in Conjugated Polymer Films for Organic Solar Cells. *Polymers (Basel).* **2016**, *8* (1), 14.

(45) Lewis, A. J.; Ruseckas, A.; Gaudin, O. P. M.; Webster, G. R.; Burn, P. L.; Samuel, I. D. W. Singlet Exciton Diffusion in MEH-PPV Films Studied by Exciton-Exciton Annihilation. *Org. Electron. physics, Mater. Appl.* **2006**, *7* (6), 452–456.

(46) Collado-Fregoso, E.; Bou, P.; Fei, Z.; Gann, E.; Ashraf, S.; Li, Z.; Mcneill, C. R.; Durrant, J. R.; Heeney, M. Increased Exciton Dipole Moment Translates into Charge-Transfer Excitons in Thiophene-Fluorinated Low-Bandgap Polymers for Organic Photovoltaic Applications. *Chem. Mater.* **2015**, *27*, 7934–7944.

(47) Faist, M. A.; Shoaee, S.; Tuladhar, S.; Dibb, G. F. A.; Foster, S.; Gong, W.; Kirchartz, T.; Bradley, D. D. C.; Durrant, J. R.; Nelson, J. Understanding the Reduced Efficiencies of Organic Solar Cells Employing Fullerene Multiadducts as Acceptors. *Adv. Energy Mater.* **2013**, *3* (6), 744–752.

(48) Groves, C. Suppression of Geminate Charge Recombination in Organic Photovoltaic Devices with a Cascaded Energy Heterojunction. *Energy Environ. Sci.* **2013**, *6* (5), 1546.

(49) Piersimoni, F.; Chambon, S.; Vandewal, K.; Mens, R.; Boonen, T.; Gadisa, A.; Izquierdo,

M.; Filippone, S.; Ruttens, B.; D'haen, J.; Martin, N.; Lutsen, L.; Vanderzande, D.; Adriaensens, P.; Manca, J. V. Influence of Fullerene Ordering on the Energy of the Charge-Transfer State and Open-Circuit Voltage in Polymer:fullerene Solar Cells. *J. Phys. Chem. C* **2011**, *115* (21), 10873–10880.

(50) Tumbleston, J. R.; Yang, L.; You, W.; Ade, H. Morphology Linked to Miscibility in Highly Amorphous Semi-Conducting Polymer/fullerene Blends. *Polymer (Guildf).* **2014**, *55* (19), 4884–4889.

(51) Tautz, R.; Da Como, E.; Limmer, T.; Feldmann, J.; Egelhaaf, H.-J.; von Hauff, E.; Lemaur, V.; Beljonne, D.; Yilmaz, S.; Dumsch, I.; Allard, S.; Scherf, U. Structural Correlations in the Generation of Polaron Pairs in Low-Bandgap Polymers for Photovoltaics. *Nat. Commun.* **2012**, *3*, 970.